The Characterization of Deep Convective Clouds as an Invariant Calibration Target and as a Visible Calibration Technique

David R. Doelling, Daniel Morstad, Benjamin R. Scarino, Rajendra Bhatt, and Arun Gopalan

***Abstract*—Deep convective clouds (DCCs) are ideal visible calibration targets because they are bright nearly isotropic solar reflectors located over the tropics and they can be easily identified using a simple infrared threshold. Because all satellites view DCCs, DCCs provide the opportunity to uniformly monitor the stability of all operational sensors, both historical and present. A collective DCC anisotropically corrected radiance calibration approach is used to construct monthly probability distribution functions (PDFs) to monitor sensor stability. The DCC calibration targets were stable to within 0.5% and 0.3% per decade when the selection criteria were optimized based on Aqua MODerate Resolution Imaging Spectroradiometer 0.65-μm-band radiances. The Tropical Western Pacific (TWP), African, and South American regions were identified as the dominant DCC domains. For the 0.65-μm band, the PDF mode statistic is preferable, providing 0.3% regional consistency and 1% temporal uncertainty over land regions. It was found that the DCC within the TWP had the lowest radiometric response and DCC over land did not necessarily have the highest radiometric response. For wavelengths greater than 1 μm, the mean statistic is preferred, and land regions provided a regional variability of 0.7% with a temporal uncertainty of 1.1% where the DCC land response was higher than the response over ocean. Unlike stratus and cirrus clouds, the DCC spectra were not affected by water vapor absorption.**

***Index Terms*—Aqua MODerate Resolution Imaging Spectroradiometer (MODIS), deep convective clouds (DCCs), pseudoinvariant calibration targets, visible imager calibration.**

I. Introduction

THERE are over 30 years of archived historical satellite imager radiances that can be used to retrieve cloud, vegetation, and aerosol properties. These data can be used for long-term climate research if all the instruments are well calibrated and data qualities across them are similar. Numerous operational geostationary Earth-observing (GEO) and polar-orbiting satellite imagers do not have onboard visible calibration. For these sensors, vicarious or postlaunch calibration is needed to monitor the sensor degradation over time. However, nearly all GEO and polar-orbiting instruments are provided with infrared (IR) imager radiances that are calibrated using onboard blackbodies. There have been many attempts to calibrate historical visible sensors, which generally followed two approaches. The first approach relies on the calibration transfer of a well-calibrated reference instrument, using boresighted coincident radiances, based on either satellite or aircraft platforms. The second approach relies on well-characterized invariant targets, such as deserts, ice sheets, clear-sky oceans, or the moon, to predict the imager radiance. Unfortunately, neither of these approaches can be applied uniformly across all operational satellites. However, deep convective clouds (DCCs) are an invariant Earth target viewed by all satellites, and they can be characterized using a well-calibrated satellite sensor. DCCs have the potential to be used as a consistent and robust calibration technique to calibrate all historical, current, and future satellite imagers.

DCCs are ideal invariant Earth targets because they are the brightest targets, are common in the tropics, and migrate seasonally with the sun, thus making them optimal solar reflectors. They have the highest signal-to-noise ratio of any Earth target, are nearly isotropic under nonoblique viewing and illumination conditions, and are located at the tropopause, where the radiative impact of atmospheric water vapor absorption, aerosols, and surface albedo is minimal. As a result, DCCs exhibit a nearly flat spectral response. They are easily identified using a simple IR threshold because they are the coldest targets in the tropics. Absolute navigation is not required; however, good IR and visible coregistration is needed for DCC target identification.

One of the first attempts to use bright clouds as a calibration reference was by Abel [1]. He used a radiative transfer model, anchored by ground-site instrumentation, to predict the National Oceanic and Atmospheric Administration (NOAA) Advanced Very High Resolution Radiometer (AVHRR) radiances of bright uniform clouds during satellite overpasses. Over the years, the predicted satellite radiances of bright clouds have been greatly improved. Ham and Sohn [2] and Okuyama [3] used MODerate Resolution Imaging Spectroradiometer (MODIS) cloud retrievals to predict coincident GEO radiances. Radiative transfer model calculations are then used to estimate the band-specific radiances. These techniques rely on MODIS cloud retrievals and, therefore, the MODIS calibration as a reference. Govaerts *et al.* [4] utilized operational Meteosat cloud products, identifying DCC by cloud height, to show that

Manuscript received February 29, 2012; revised July 3, 2012; accepted September 4, 2012. Date of publication December 10, 2012; date of current version February 21, 2013. This work was supported by the NASA CERES program, the NASA Satellite Intercalibration Consistency program, and the NOAA NCDC SDS Climate Data Records program IA1-1016.

D. R. Doelling is with the Climate Science Branch, Langley Research Center, National Aeronautics and Space Administration, Hampton, VA 23681 USA (e-mail: david.r.doelling@nasa.gov).

D. Morstad, B. R. Scarino, R. Bhatt, and A. Gopalan are with Science Systems and Applications, Inc., Hampton, VA 23666 USA (e-mail: Daniel.morstad@nasa.gov; Benjamin.r.scarino@nasa.gov; rajendra.bhatt@nasa.gov; arun.gopalan-1@nasa.gov).

Digital Object Identifier 10.1109/TGRS.2012.2225066

DCCs were radiatively invariant when the cloud optical depth exceeds 100. They then used an *a priori* model to predict the Meteosat visible radiance.

The first DCC calibration technique, which used the collective DCC pixel-level radiances over the month, was by Hu *et al.* [5]. They evaluated the stability of the Clouds and the Earth's Radiant Energy System (CERES) broadband (BB) short-wave fluxes and the Visible and Infrared Scanner (VIRS) and MODIS visible radiances on board the Tropical Rainfall Measuring Mission (TRMM) and Terra satellites, respectively. A simple IR threshold was used to identify DCC pixels, and the DCC TRMM angular distribution model (ADM) was applied to the CERES fluxes, whereas a nonlinear-regression neural-network-based BB-to-narrow-band (NB) conversion was applied for the visible imagers. The DCC monthly VIRS or MODIS albedo distribution was within 1%. Using the same technique, Doelling *et al.* [6] used a simple IR threshold and the CERES DCC BB bidirectional reflectance distribution function (BRDF) to determine the relative temporal degradation of AVHRR on board the NOAA-16 and NOAA-17 satellites. Aumann *et al.* [7], using an IR threshold of 210 K and assuming a Lambertian ADM, concluded, using four years of data, that the Atmospheric Infrared Sounder (AIRS) visible channel, on board Aqua, had a stability of 0.2% per decade. Minnis *et al.* [8] improved the technique by applying a spatial homogeneity threshold, and other selection criteria, to reduce the occurrence of optically thin clouds. The DCC technique was able to identify a 1.2% relative calibration anomaly in MODIS Band-1 Collection-5 radiances on board Terra during November 2003. A slight variation of [8] was submitted as a Global Space-Based Inter-Calibration System Algorithm Theoretical Basis Document [9]. Fougnie and Bach [10] calibrated POLarization and Directionality of the Earth Reflectances (POLDER) radiances using DCC. Given that POLDER does not have an IR channel, they selected DCC based on the visible reflectance of large convective cells identified from the oxygen A-band derived cloud heights. In order to reduce the DCC BRDF modeled radiance uncertainty, Sohn *et al.* [11] selected DCC with overshooting tops. Owing to the sparse sampling of DCC when using these criteria, the temporal stability uncertainty of MODIS for this method is 5%.

The objective of this paper is to establish DCC as an invariant Earth target and apply a DCC-based calibration technique to monitor sensor stability, which can be used uniformly across all historical and current operational visible sensors to assess the sensor's on-orbit performance. This paper is organized as follows. Section II outlines the baseline DCC calibration technique applicable to most operational visible sensors. This technique is illustrated using Aqua MODIS. In Section III, individual criteria are incrementally adjusted to estimate their impact and uncertainty on the resulting DCC calibration. The fourth section characterizes the DCC natural variability, both regionally and temporally. Individual geographical regions will be evaluated to determine their viability as DCC calibration domains. This section provides the uncertainties of using the DCC technique and explains how to mitigate the uncertainties unique to each geographical satellite domain and spectral band. Conclusions are presented in Section V.

II. DCC Calibration Technique

The DCC calibration technique is a two-step process: First, identify the DCC target, and second, predict the DCC radiance over the established target. In order for this technique to be consistent across nearly all satellite imagers, only the visible-channel and single-window-channel IR pixel-level data will be used. Even though some modern sensors have multiple bands, which may increase the skill in capturing pristine DCC scenes, these may be subject to change in sensor data quality and availability over time. Rather than relying on identifying a sparse set of pristine DCC pixels based on multiple thresholds from various sources or from contemporary well-calibrated satellite data, the baseline technique will rely on the collective pixel DCC calibration approach [5]–[9] using only IR temperature and spatial uniformity thresholds that can be applied to most sensors. This procedure mitigates the impact of a selective DCC mask given that all the DCC pixel-level radiances are evaluated as a whole.

Unfortunately, there are no perfectly calibrated sensors that can flawlessly isolate the natural variability of DCC. Therefore, the reference instrument uncertainty must be included while computing the uncertainty owed to the DCC calibration technique. Wu *et al.* [12] determined Aqua-MODIS Band 1 (0.65 μm) to be better characterized and more temporally stable than that of Terra MODIS. They found Aqua MODIS to be stable to within 0.5% per decade, over the first eight years of operation. Therefore, to minimize the reference instrument uncertainty, the authors chose Aqua MODIS as a reference. All results presented in this paper are a combination of Aqua-MODIS calibration and DCC target variability over time. For this section, Collection-5 Aqua-MODIS 1-km nominal-resolution (subsampled to 2-km resolution) pixel-level Band-1 radiances and Band-31 (11 μm) brightness temperatures (BTs) between July 2002 and June 2010 (the same eight-year record) are used.

A. Baseline DCC Technique

Any pixel located over the tropical domain between 30° N and 30° S with an 11-μm BT less than 205 K is identified as a DCC pixel target. To improve the capture of only the convective core, a spatial uniformity threshold is applied by computing the spatial standard deviation of the identified pixel and its eight surrounding neighbors. Pixels with standard deviations less than 3% in the visible and 1 K in the IR are used. Only solar zenith angles (SZAs) and view zenith angles (VZAs) of less than 40° are used to take advantage of the more Lambertian part of the DCC reflectance field. The DCC anisotropically corrected (AC) radiance Rad_{AC} is computed as follows:

$$Rad_{\mathrm{AC}} = \frac{r}{\delta(d_y)\cos(\theta_0)R(\theta_0,\theta,\phi)} \tag{1}$$

where r is the DCC pixel radiance, δ is the Earth–sun distance correction factor computed for the day of the year d_y, θ_0 is the SZA, θ is the VZA, ϕ is the azimuthal angle, and R is the DCC ADM factor that is empirically derived from the MODIS radiances (described in Section III-C). The DCC AC radiance

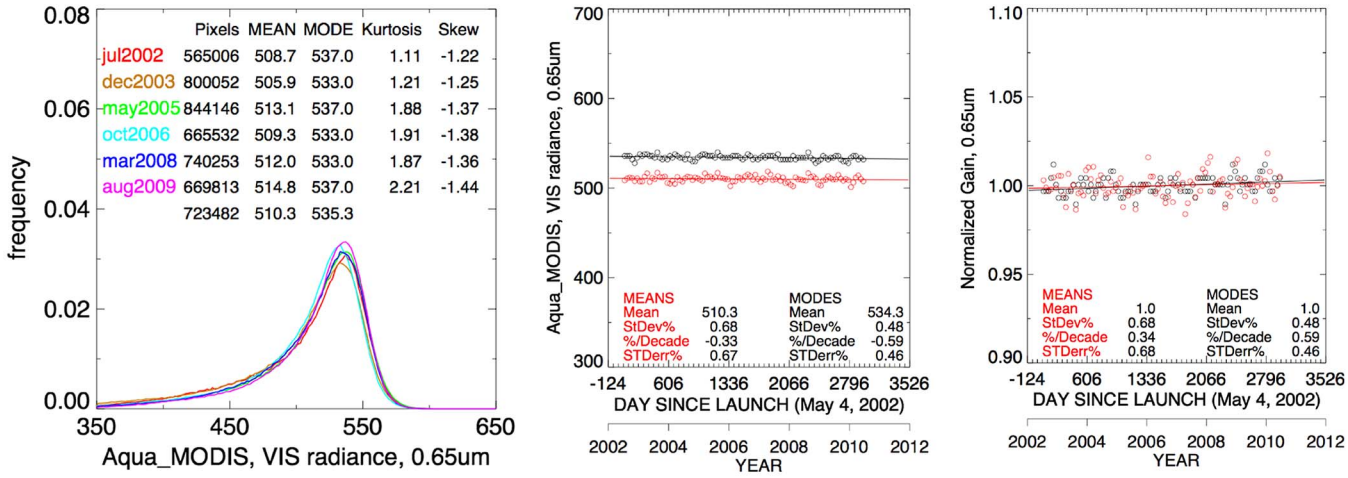

Fig. 1. (Left panel) Aqua-MODIS monthly PDF of DCC AC 0.65-μm radiance for July 2002–June 2011. (Center panel) Monthly (red) mode and (black) mean DCC AC radiances. The radiance unit is W $\cdot$ m^{-2} $\cdot$ sr^{-1} $\cdot$ μm^{-1}. (Right panel) Same as center except normalized.

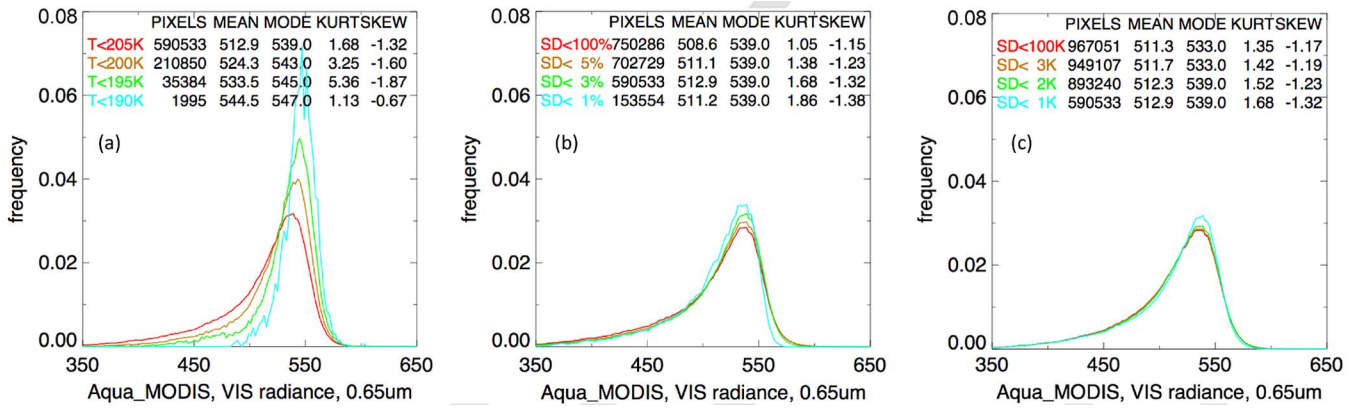

Fig. 2. Aqua-MODIS August 2004 PDF of DCC AC 0.65-μm radiances as a function of (a) temperature threshold (K), (b) visible spatial standard deviation threshold (%), and (c) IR spatial standard deviation threshold (K). The radiance unit is W $\cdot$ m^{-2} $\cdot$ sr^{-1} $\cdot$ μm^{-1}.

is dependent on the ADM factor and may not necessarily return the true DCC radiance or reflectance when divided by the band solar constant.

Monthly probability distribution functions (PDFs) are constructed, from all the DCC-identified pixel-level AC radiances, with a bin size of approximately 0.5% of the average DCC AC radiance. Fig. 1(a) shows that the monthly PDFs of DCC AC radiances are consistent from month to month as expected from a well-calibrated instrument. Over 500 000 pixels are identified monthly using this technique. The mean and mode of the DCC AC radiance, as well as the kurtosis and skewness, are similar from month to month, indicating the robustness of the method. Fig. 1(b) shows the monthly PDF mean and mode DCC AC radiances as a function of time. The DCC AC radiance monthly mean and mode standard deviations are 0.68% and 0.48%, respectively, validating the temporal invariance of the DCC target. The mode DCC AC radiance is greater than the mean due to the asymmetrical shape of the PDF. Fig. 1(c) shows the normalized inverse monthly PDF mean and mode DCC AC radiances as a function of time. The linear regression of the monthly mean and mode DCC AC radiances is consistent within 0.26% per decade, indicating that either PDF statistic can be used to evaluate the temporal stability of a sensor.

III. DCC Threshold Sensitivity and Uncertainty Analysis

The sensitivity of DCC calibration to certain thresholds and models can provide insight into the DCC calibration uncertainty. IR temperature threshold, visible-channel spatial uniformity threshold, IR spatial uniformity threshold, and anisotropic model selection effects can all be evaluated by comparing the baseline method results to the results found when each individual criterion was independently varied.

A. IR Temperature Threshold

The first criterion is to investigate the IR 11-μm temperature threshold, used as the basis to identify DCC. Previous studies [5], [7], [8], [11] used IR temperature thresholds between 190 K and 210 K in an attempt to identify bright uniform DCC targets. To determine the effect of the temperature threshold on the shape of the DCC AC radiance PDF, the threshold was incremented by 5 K between 190 K and 205 K for August 2004 [shown in Fig. 2(a)]. A 2% (0.5%) increase in the mean (mode) PDF with each 5-K decrease in the temperature threshold is apparent. The advantage of using a lower temperature threshold is

TABLE I
AVERAGE MODE AND MEAN AQUA-MODIS DCC AC RADIANCES FOR JULY 2002–JUNE 2010 AS A FUNCTION OF TEMPERATURE THRESHOLD. THE ASSOCIATED MONTHLY MODE (TEMPORAL) STANDARD DEVIATION AND TREND ARE ALSO GIVEN

Temperature Threshold (K)	Mode DCC radiance ($Wm^{-2}sr^{-1}\mu m^{-1}$)	Mean DCC radiance ($Wm^{-2}sr^{-1}\mu m^{-1}$)	Monthly Mode standard deviation (%)	Mode trend (%/decade)
205	534.3	510.3	0.48	-0.57
200	537.7	521.2	0.48	-0.53
195	541.2	530.9	0.50	-0.56
190	545.0	539.9	0.78	-0.76
185	548.5	549.5	1.30	-0.44
180	553.3	554.5	1.11	1.39

TABLE II
AVERAGE MODE AND MEAN AQUA-MODIS DCC AC RADIANCES FOR JULY 2002–JUNE 2010 AS A FUNCTION OF PIXEL 0.65-μm RADIANCE (SPATIAL) STANDARD DEVIATION. THE ASSOCIATED MONTHLY MODE (TEMPORAL) STANDARD DEVIATION AND TREND ARE ALSO GIVEN

0.65μm StDev threshold (%)	Mode DCC radiance ($Wm^{-2}sr^{-1}\mu m^{-1}$)	Mean DCC radiance ($Wm^{-2}sr^{-1}\mu m^{-1}$)	Monthly Mode standard deviation (%)	Mode trend (%/decade)
None	533.4	505.5	0.51	-0.71
5	533.9	508.2	0.51	-0.64
3	534.3	510.3	0.48	-0.57
1	533.4	510.8	0.54	-0.88

TABLE III
AVERAGE MODE AND MEAN AQUA-MODIS DCC AC RADIANCES FOR JULY 2002–JUNE 2010 AS A FUNCTION OF PIXEL 11-μm BT (SPATIAL) STANDARD DEVIATION. THE ASSOCIATED MONTHLY MODE (TEMPORAL) STANDARD DEVIATION AND TREND ARE ALSO GIVEN

11μm StDev Threshold (K)	Mode DCC radiance ($Wm^{-2}sr^{-1}\mu m^{-1}$)	Mean DCC radiance ($Wm^{-2}sr^{-1}\mu m^{-1}$)	Monthly Mode standard deviation (%)	Mode trend (%/decade)
None	532.8	509.3	0.51	-0.67
3	532.8	509.5	0.52	-0.69
2	533.0	509.9	0.51	-0.70
1	534.3	510.3	0.48	-0.57

the reduction of the number of dark-pixel radiances to the left of the PDF peak. The PDF kurtosis, which quantifies the peakedness, increases, confirming that a lower temperature threshold targets only DCC clouds rather than thick cirrus conditions, the latter of which is usually associated with the convective anvil. However, the colder threshold dramatically reduced the DCC sample size. A 94% reduction in DCC frequency was observed when reducing the threshold from 205 K to 195 K. The 190-K threshold produced a very noisy PDF owing to the lack of DCC samples.

The main objective of the temperature threshold is to capture consistent monthly PDFs. Table I provides the relationship of the temperature threshold and the eight-year monthly PDF mode standard deviation. For Aqua MODIS, a temperature threshold between 205 K and 195 K produced similar PDF mode temporal variability. However, for thresholds less than 195 K, the temporal variability increases significantly owing to the lack of sampling. Fig. 2(a) and Table I show a similar increase in mean and mode DCC AC radiances with decreasing temperature threshold, but this dependence does not impact the temporal trend or variability. It seems that, as long as the DCC sample size is sufficient, the temperature threshold is somewhat arbitrary. Therefore, the only IR calibration requirement is temporal stability, not absolute calibration. Most operational imagers over the last 30 years are calibrated using an onboard blackbody, which assures the temporal stability of the IR calibration needed for this technique [13].

B. Spatial Uniformity Thresholds

Spatial uniformity tests tend to increase the accuracy of identifying only DCC cells [8], [11]. Fig. 2(b) and (c) shows the monthly PDF for August 2004 as a function of various visible and IR standard deviation thresholds, respectively. There is only a slight increase in the kurtosis, or peakedness, but at the expense of sample size. The visible spatial threshold is slightly more effective in defining a sharp PDF peak than the IR spatial threshold, but neither is as effective as temperature. Tables II and III show that the PDF mode temporal variability is not affected by either visible or IR spatial threshold; however, there is a weak increase in the PDF mode and mean radiances when applying stricter spatial thresholds. In practice, the temperature threshold is usually determined first by examining monthly PDFs over the year and then enhanced by using the spatial uniformity test if there is sufficient sampling available. Having very restrictive thresholds severely reduces the number of DCC samples, results in ambiguous PDF modes, and thus reduces the success of this technique.

C. Anisotropic Correction

The last component to investigate is the anisotropic correction of the DCC pixel radiance. In order to infer the uncertainty associated with the ADM, four DCC ADMs are considered. The first ADM assumes that DCCs are perfect Lambertian diffuse reflectors, and therefore, no anisotropic correction is

needed. Aumann *et al.* [7] reported that AIRS visible channels were calibrated within 0.2% per decade using a Lambertian ADM. The second is the 0.65-μm ADM based on a nonlinear neural-network-based regression by Hu *et al.* [5] which converts the BB CERES DCC ADM to NB. The third is the TRMM CERES BB DCC ADM [14]. The fourth is the Aqua-MODIS ADM, which was developed by angularly binning the DCC reflectances [(1), replacing the ADM factor with the Aqua-MODIS solar constant] over the first three years of Aqua (July 2002–June 2005), which is the most stable portion of the record (Jack Xiong, personal communication). The same DCC selection criteria used to construct an ADM should be used to apply the ADM, not to bias the results. When constructing the MODIS-based ADM, the average angular bin radiance divided by the MODIS solar constant of 509.3 $\mathrm{W \cdot m^{-2} \cdot sr^{-1} \cdot \mu m^{-1}}$ is used as the anisotropic correction factor. If a DCC pixel is identified with an angular bin that is not associated with an ADM factor, it is not used. It is important when deriving a sensor-specific ADM to use at least a year's worth of data, thus ensuring sufficient angular bin coverage. A maintained polar or GEO orbit, and the assumption that the spatial and temporal coverage of DCC is expected to be consistent from year to year, allows the construction of a sensor-specific ADM during the time period when the on-orbit sensor dependences are best understood.

Comparing the DCC AC PDF radiances as a function of both ADM type and viewing geometry is an excellent way to validate the DCC PDFs, as shown in Fig. 3. If the DCC ADM factors were perfect, all of the angularly varied PDFs would be identical. As expected, the Aqua-MODIS ADM shows the best agreement, whereas the Lambertian ADM shows the least uniformity. Even if no ADM is applied, the DCC radiance ranges across all of the SZA, VZA, and azimuth angle (AZA) bins are 35% and 5% of the PDF mean and mode, respectively, thereby verifying that DCCs are near-perfect solar reflectors and excellent invariant Earth targets. Table IV displays the monthly DCC mode temporal variability, and the associated trend is shown as a function of ADM. The monthly standard deviation ranges between the three DCC-specific ADMs are within 0.11, and within 0.30% when including the Lambertian case. The associated trend ranges are 0.30% and 0.59% per decade without and with the Lambertian case, respectively. Given that the DCC geographical and seasonal distribution is similar from year to year and that the satellite orbit is well maintained and not allowed to degrade, it follows that the DCC angular reflectance is invariant. The Lambertian ADM was used to illustrate the near isotropic behavior of DCC under nonoblique viewing and solar illumination conditions; however, it is recommended to use a sensor-specific ADM to optimize the results of this technique. If a sensor-specific ADM is not available, it is then advisable to use a generic DCC ADM.

IV. DCC Target Characterization

The DCC calibration technique is only as good as the invariance of the DCC target. Yuan and Li [15] state that there is little DCC interannual variability over a given region but there is geographic variability in particle size and optical depth based on MODIS cloud retrievals. Smaller particle sizes are more reflective than larger particles and are a function of the cloud-top temperature. The variation of the DCC microphysics, during the DCC life cycle and by the regional convective dynamics, needs to be investigated. In this section, DCC AC radiance natural variability is examined temporally, spatially, and spectrally. If the DCC radiances show any dependences or large natural oscillations as a function of geography or spectral response, the DCC calibration technique could take this into account by either limiting the DCC identification to certain conditions or by correcting for them.

A. Aqua-MODIS DCC Regional Frequency

In order for DCC calibration to be successful, DCC must be present over the calibration domain during the sampling time of the sensor, the DCC frequency must be consistent interannually, and the DCC must not be trending in time. Hong *et al.* [16] have shown that the 1995–2003 combined 7:00 and 19:00 local-time tropical DCC coverage is $\sim$0.5% and the associated cloud amount stability is -3% per decade based on microwave measurements. They also show that DCCs migrate seasonally with the sun and that the DCC frequency peaks in the late afternoon (morning) over land (water). The objective of this section is to identify which 10°-by-10° geographical regions have enough DCC samples for successful calibration. These regions do not necessarily require DCC every month but enough sampled months during the year to establish the temporal stability. The frequency analysis is based on a 13:30 local equator crossing time given that the same Aqua-MODIS data set is used in this section. The DCC technique is refined by only incorporating months with more than 3000 DCC pixels, only using regions that include a minimum of 30 months, and by using an optimized PDF binning technique [17], which tends to increase the bin size of the PDF if the data for a given region in a given month are sparse. A combination of temperature and spatial uniformity threshold adjustments of the baseline technique is analyzed and shown.

There are three dominant DCC domains where DCCs occur almost every month: the Tropical Western Pacific (TWP), equatorial Africa, and South America (Fig. 4). The rest of the domains have seasonally active DCC. When no spatial threshold is applied, the number of viable DCC regions is reduced by 35% and 75% when the temperature threshold is reduced from 205 K to 200 K and 195 K, respectively. Only these dominant domains have sufficient DCC sampling at the 195-K threshold. The application of the spatial threshold has approximately reduced the DCC geographical frequency in the same manner as reducing the temperature threshold by 5 K (Fig. 4).

B. Aqua-MODIS Radiances Stratified Regionally, Temporally, and by Band

For the viable regions meeting the minimum regional frequency thresholds, the eight-year DCC AC 0.65-μm radiance PDF mean and mode, using the 205-K threshold without the spatial threshold, are computed and are shown in Fig. 5. The regional standard deviations are 0.8% and 1.4% for the mode and the mean, respectively, and are shown in Table V under

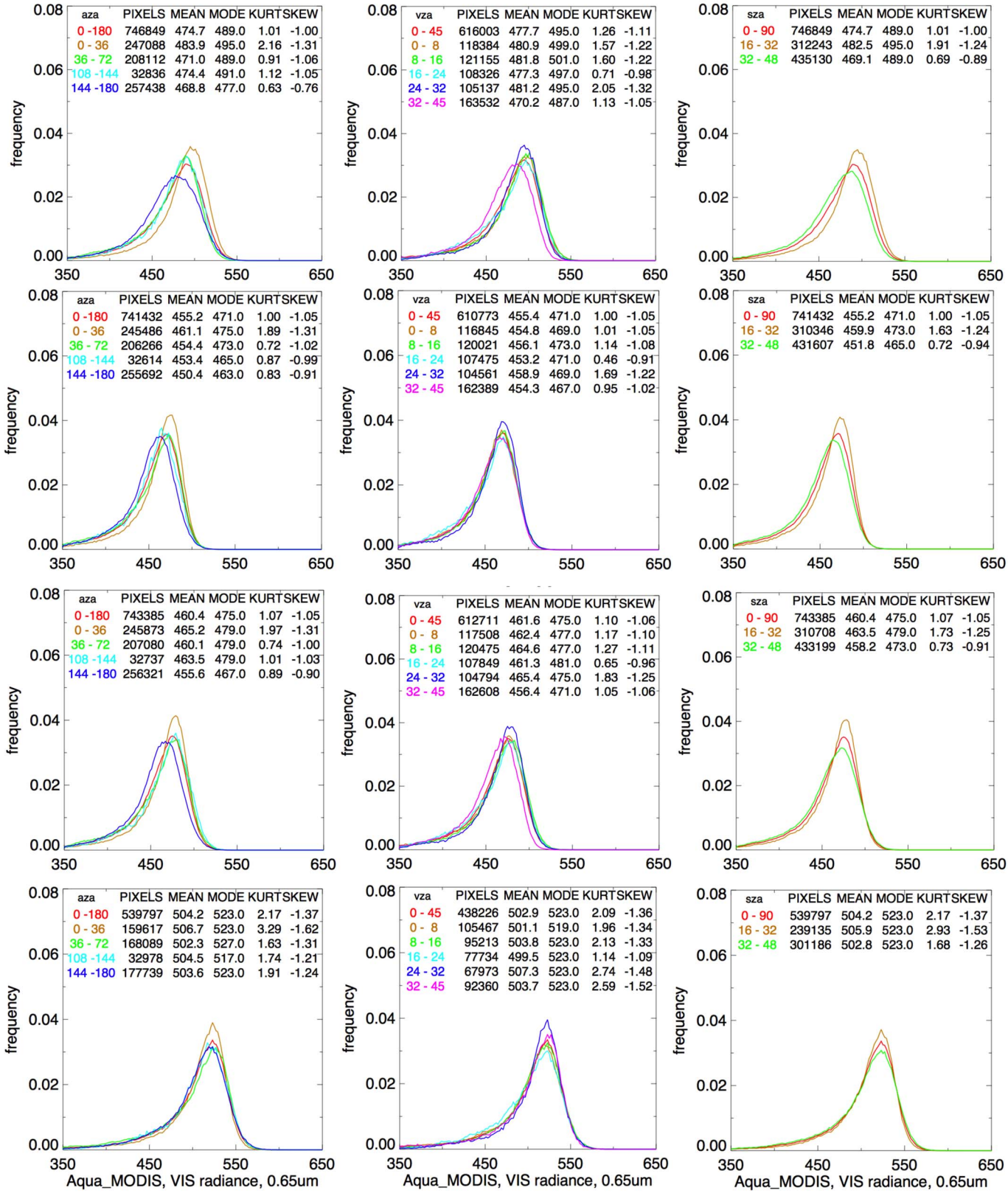

Fig. 3. Aqua-MODIS August 2004 PDF of DCC AC 0.65-μm radiances as a function DCC ADM type: (Top row) Lambertian ADM, (second row) ADM by Hu *et al.* [5], (third row) CERES ADM [11], and (bottom row) MODIS ADM. (Left column) AZA, (center column) VZA, and (right column) SZA in degrees. The radiance unit is $\mathrm{W} \cdot \mathrm{m}^{-2} \cdot \mathrm{sr}^{-1} \cdot \mu\mathrm{m}^{-1}$.

the "spatial" column. The regional eight-year monthly standard deviations of the mode and mean are shown in Fig. 5. The average of all the regional monthly standard deviations is given in Table V under the "month" column. Similarly, the average annual standard deviation is computed and also shown in Table V and is at least half of the monthly standard deviation.

TABLE IV
MONTHLY AQUA-MODIS DCC AC MODE RADIANCE (TEMPORAL) STANDARD DEVIATION AND TREND AS FUNCTIONS OF ADM TYPE FOR JULY 2002–JUNE 2010

ADM	Monthly Mode standard deviation (%)	Trend (%/decade)
Lambertian	0.67	-0.86
Hu (theory)	0.37	-0.51
CERES (BB)	0.46	-0.27
MODIS (NB)	0.48	-0.57

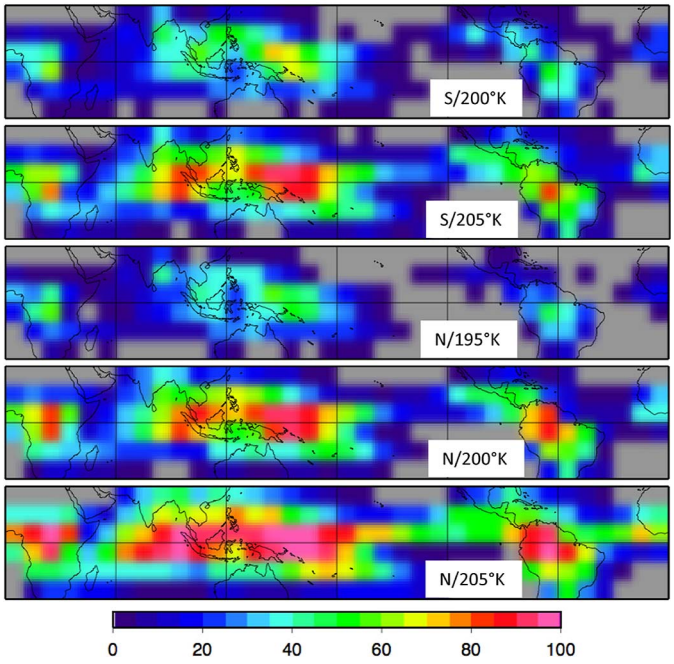

Fig. 4. Number of months with an Aqua-MODIS DCC pixel count greater than 3000 over 10°-by-10° latitude/longitude regions for July 2002–June 2010 as a function of spatial and temperature thresholds. The *S* indicates that the spatial thresholds were applied, and *N* indicates that no thresholds were applied.

It is apparent for the 0.65-μm band that the PDF mode statistic is more uniform regionally than the mean statistic.

The highest DCC radiances are not necessarily over land, but the lowest DCC radiances are consistently found over the TWP. The Africa and South America domains are more temporally stable than regions over most of the TWP. For the tropics as a whole, reducing the temperature threshold is more effective than using stricter spatial thresholds in reducing the monthly uncertainty for an equivalent number of viable regions. The differences between the temperature and spatial thresholds are more similar over land than over ocean. This suggests that land convection is more diurnally consistent geographically than over oceans, the former where geographical and multiple convection dynamics are in place [18]. In order to capture the peak of the convective life cycle over the ocean, the proper temperature threshold is necessary. This results in land-based DCC having lower regional and temporal uncertainties than ocean-based DCC with the use of this technique.

Table V indicates that the DCC calibration technique can achieve a 10°-by-10° regional consistency of 0.3% and a temporal uncertainty of 1% over the dominant land domains using the mode statistic for the 0.65-μm band. Over the tropics, this regional consistency is elevated to 0.5% with a temporal uncertainty of 1.3%. Nevertheless, this is as good as the temporal uncertainty of the best desert sites–:$\sim$1% [12], [19]. However, when the tropics are analyzed on an annual basis, the temporal uncertainty is reduced to 0.6%, nearly half that of the desert sites. Tables VI and VII show that the MODIS bands with wavelengths less than 0.65 μm behave in the same fashion as the 0.65-μm band. Unfortunately, the MODIS 0.86-μm band saturates over DCC and cannot be evaluated. All MODIS bands reveal that the interannual variability is half of the monthly variability.

For the MODIS 2.12-μm band, there is a distinct regional DCC radiance difference between land and water surfaces, with the land having a brighter DCC AC radiance, as shown in Fig. 6. The brighter land radiances indicate that the particle sizes are smaller over land than over ocean. However, the 3.6% spatial variability based on the PDF mode statistic is reduced by about half, compared to the mean statistic of 2.0%, as shown in Table VI, for the 205-K temperature threshold. The PDF mean statistic also reduces the temporal variation significantly over ocean surfaces. Land regions surprisingly have temporal variations less than 1% when using the mean statistic. The MODIS 2.12-μm band was designed to aid in particle size retrieval. This knowledge suggests that the 2.12-μm band can be calibrated using this technique if it is limited to the dominant land regions. Table VII reveals that, for the PDF mean statistic, the monthly variation is 1.1% and is spatially consistent within 0.7% over land. Table VII also reveals that the other MODIS bands with wavelengths greater than 1 μm have similar characteristics to the 2.12-μm band.

C. SCIAMACHY and Hyperion Hyperspectral DCC Reflectances

Bright clouds have been used as a calibration transfer medium to cross-calibrate aircraft and satellite radiances. Vermote and Kaufman [20] used bright optically thick clouds to transfer the calibration of AVHRR 0.65-μm band to the 0.86-μm band by assuming that the reflectance ratio was constant for BTs less than 225 K, owing to the lack of water vapor absorption in the near IR. Lafrance *et al.* [21] used tropical cumulonimbus clouds to transfer the calibration of one POLDER channel to another using predetermined simulations of ice clouds, which was more successful than using low-level bright stratus clouds. This section describes the use of SCanning Imaging Absorption SpectroMeter for Atmospheric CartograpHY (SCIAMACHY) V.7.01 level-1B spectrum reflectances [22]–[24] on board the Envisat satellite, which has a local equator crossing time of 10:00 A.M., in transferring calibration. At 1-s integration time, SCIAMACHY has a footprint size of 30 km by 240 km and a spectral resolution between 0.2 and 0.5 nm over a wavelength range from 240 to 1700 nm. In order to determine the cloud conditions of the SCIAMACHY footprint, nearly coincident (within 30 min) Terra-MODIS cloud retrievals from the CERES Single Scanner Footprint level-2 20-km product [25] were obtained for the center and each of the four corners of the SCIAMACHY footprint.

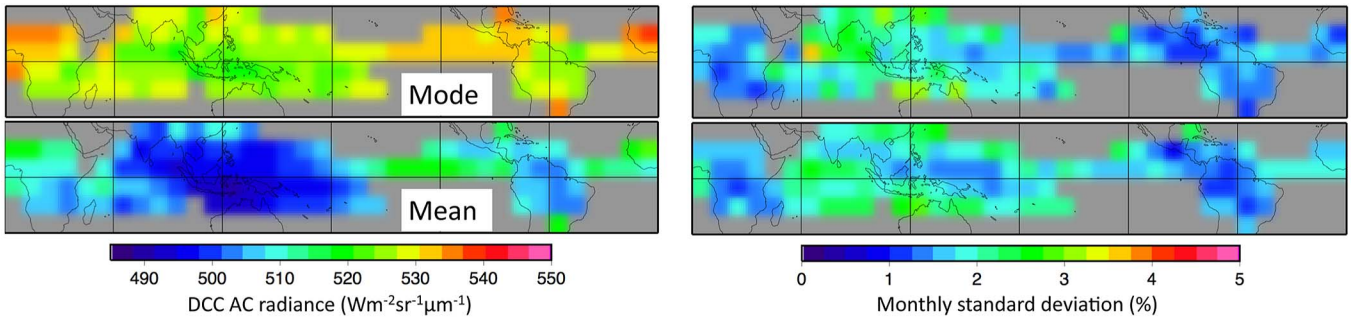

Fig. 5. (Left panels) Mean regional Aqua-MODIS DCC 0.65-μm-band radiance for the mode and mean statistics. (Right panels) Monthly (temporal) standard deviation using the baseline technique without applying spatial threshold.

TABLE V

MONTHLY AQUA-MODIS DCC AC 0.65-μm MEAN AND MODE RADIANCE SPATIAL (10° -BY-10° LATITUDE/LONGITUDE REGIONS), MONTHLY, AND ANNUAL STANDARD DEVIATIONS FOR JULY 2002–JUNE 2010 AS A FUNCTION OF SURFACE TYPE AND SPATIAL AND TEMPERATURE THRESHOLDS. THE *Y* INDICATES THAT THE SPATIAL THRESHOLDS WERE APPLIED. # INDICATES THE NUMBER OF REGIONS PRESENT UNDER EACH METHOD. *Tropics* INCLUDE ALL REGIONS BETWEEN ±30° IN LATITUDE, AND *Land* DENOTES THE AFRICAN AND AMERICAN CONTINENTS WITHIN THE TROPICS

0.65μm	Threshold			MODE			MEAN		
Surface	Temp (K)	Spatial	#	Spatial (%)	Month (%)	Annual (%)	Spatial (%)	Month (%)	Annual (%)
Tropics	205		117	0.8	1.8	0.7	1.4	1.8	0.8
	205	Y	78	0.6	1.6	0.7	1.5	1.9	0.9
	200		78	0.6	1.4	0.6	1.2	1.6	0.7
	200	Y	43	0.5	1.2	0.6	1.1	1.6	0.8
	195		27	0.5	1.3	0.7	1.0	1.4	0.8
Land	205		29	0.8	1.5	0.6	1.1	1.5	0.6
	205	Y	22	0.5	1.1	0.5	0.7	1.4	0.7
	200		24	0.6	1.3	0.6	0.9	1.3	0.6
	200	Y	11	0.3	1.0	0.5	0.3	1.2	0.6
	195		8	0.3	1.1	0.5	0.3	1.1	0.6

TABLE VI

BASELINE WITHOUT THE APPLIED SPATIAL THRESHOLD MONTHLY AQUA-MODIS DCC AC 0.65-μm MEAN AND MODE RADIANCE SPATIAL (10°-BY-10° LATITUDE/LONGITUDE REGIONS), MONTHLY, AND ANNUAL STANDARD DEVIATIONS FOR JULY 2002–JUNE 2010 AS A FUNCTION OF MODIS BAND AND SURFACE. *Tropics* INCLUDE ALL REGIONS BETWEEN ±30° IN LATITUDE, AND *Land* DENOTES THE AFRICAN AND AMERICAN CONTINENTS WITHIN THE TROPICS

Tropics/Land	MODE			MEAN		
MODIS BAND (μm)	Spatial (%)	Month (%)	Annual (%)	Spatial (%)	Month (%)	Annual (%)
1 (0.65)	0.5/0.3	1.2/1.0	0.6/0.5	1.1/0.3	1.6/1.2	0.8/0.6
3 (0.47)	0.5/0.4	1.3/1.1	0.6/0.5	1.1/0.3	1.7/1.2	0.8/0.5
4 (0.55)	0.5/0.3	1.3/1.1	0.6/0.5	1.1/0.3	1.7/1.2	0.8/0.6
5 (1.24)	1.2/0.7	1.3/1.0	0.6/0.5	1.3/0.7	1.0/0.8	0.5/0.4
6 (2.12)	2.5/1.2	3.4/1.9	2.0/1.7	1.8/0.7	1.8/1.1	1.1/1.0
26 (1.37)	2.0/1.1	2.7/1.9	1.2/0.9	2.3/0.9	2.0/1.5	1.0/0.6

TABLE VII

BASELINE WITHOUT THE APPLIED SPATIAL THRESHOLD MONTHLY AQUA-MODIS DCC AC 0.65-μm MEAN AND MODE RADIANCE SPATIAL (10°-BY-10° LATITUDE/LONGITUDE REGIONS), MONTHLY, AND ANNUAL STANDARD DEVIATIONS FOR JULY 2002–JUNE 2010 AS A FUNCTION OF MODIS BAND AND TEMPERATURE THRESHOLD

205 K/195 K	MODE			MEAN		
MODIS BAND (μm)	Spatial (%)	Month (%)	Annual (%)	Spatial (%)	Month (%)	Annual (%)
1 (0.65)	0.8/0.5	1.8/1.3	0.7/0.7	1.4/1.0	1.8/1.4	0.8/0.8
3 (0.47)	0.8/0.6	1.8/1.4	0.7/0.7	1.7/1.1	2.1/1.4	0.9/0.7
4 (0.55)	0.8/0.6	1.9/1.3	0.8/0.6	1.6/1.1	2.1/1.4	0.9/0.8
5 (1.24)	1.5/1.3	1.5/1.2	0.7/0.6	1.4/1.1	1.1/0.9	0.5/0.5
6 (2.12)	3.6/2.6	3.6/3.1	1.7/2.0	2.0/1.2	1.9/1.6	0.9/1.0
26 (1.37)	2.9/1.7	3.4/1.8	1.6/0.9	2.8/1.6	2.4/1.3	1.1/0.7

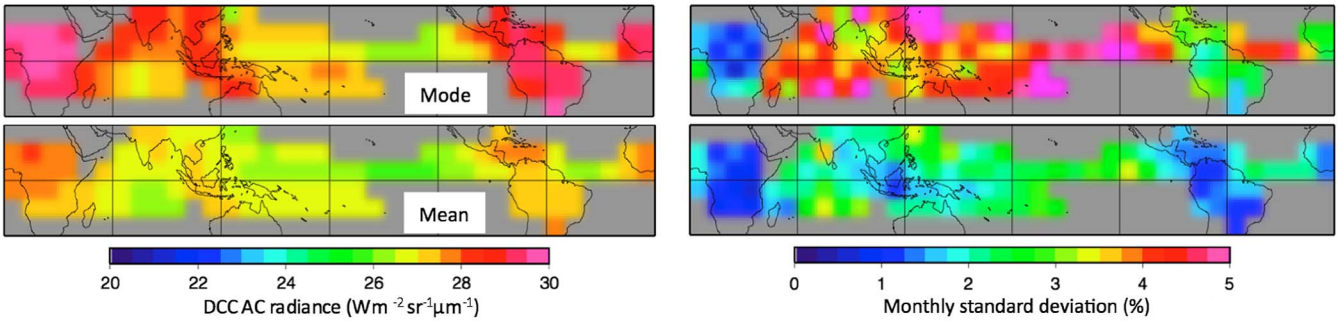

Fig. 6. Same as Fig. 5 except for the Aqua-MODIS 2.12-μm band.

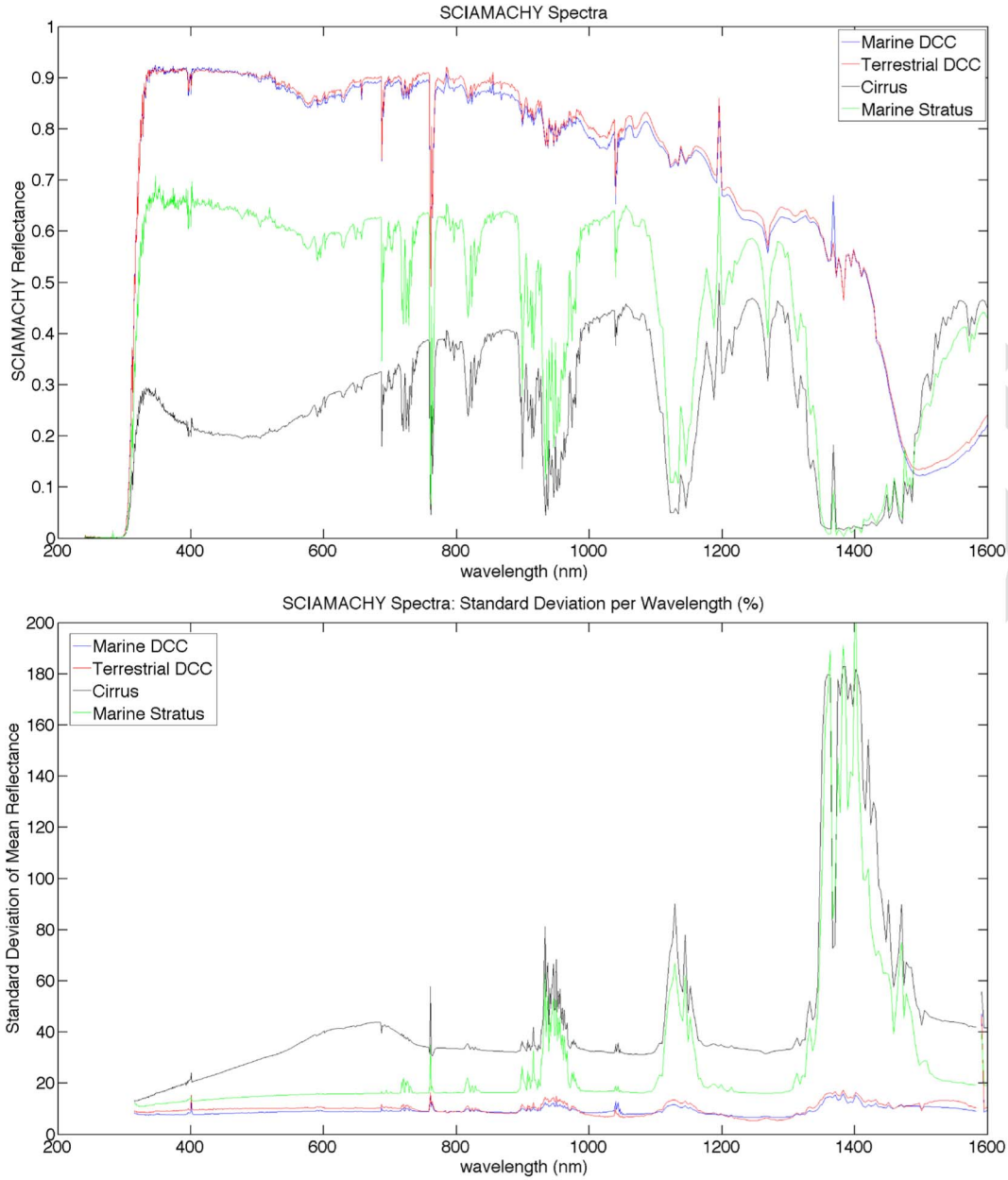

Fig. 7. (Top panel) Mean SCIAMACHY footprint reflectances over (red line) DCC land, (blue line) DCC ocean, (green line) cirrus, and (black line) maritime stratus. (Bottom panel) Standard deviation of the SCIAMACHY footprint reflectances in percent.

Four cloud conditions were isolated from the collection of SCIAMACHY footprints within $\pm 30^{\circ}$ in latitude between August 2002 and December 2010. The cloud fraction of the center footprint location must be at least 99%, and the corners report a cloud fraction greater than 1%. A footprint is considered land if the center location (20 km) has land coverage

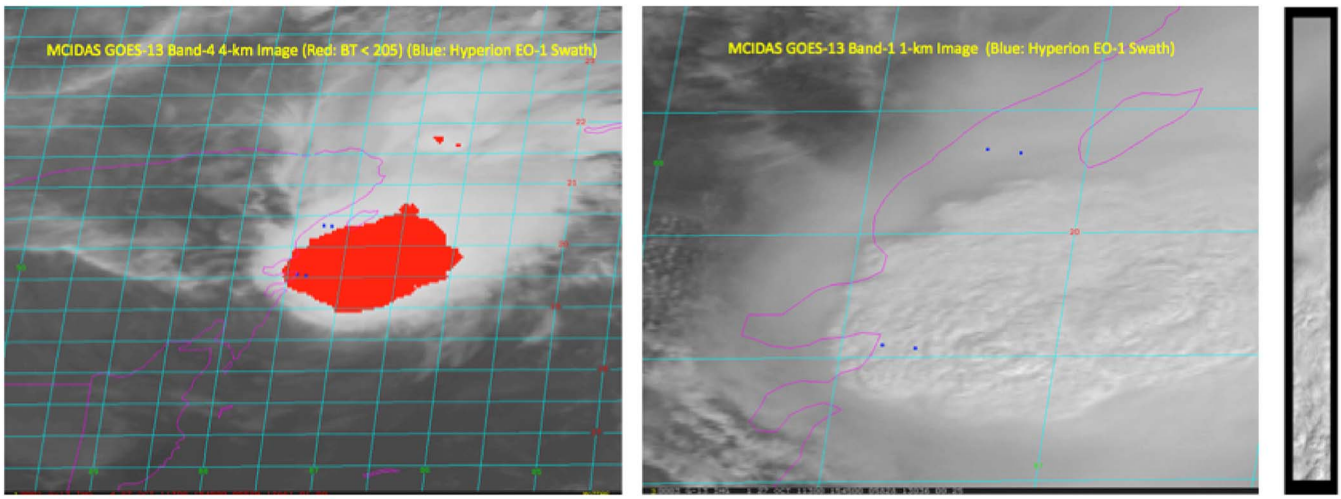

Fig. 8. (Left panel) October 27, 2011, GOES-13 IR (4 km) 15:45 GMT image. BTs less than 205 are shaded in red. The blue dots demarcate the four corners of the Hyperion image. (Center panel) October 27, 2011, GOES-13 visible (1 km) 15:45 GMT image. (Right panel) Corresponding EO1-Hyperion (EO1H0180462011300110KF_SGS_01) 600-nm image.

greater than 90% and the corners contain land and vice versa for ocean. A footprint is classified as DCC if the cloud-top temperature is less than 205 K and the optical depth is greater than 70 at the center location. If the center footprint location has a cloud-top temperature less than 205 K and an optical depth less than five, it is classified as a cirrus cloud. A footprint is identified as stratus if the cloud-top temperature is greater than 270 K and the optical depth is greater than 20 for the center location.

Fig. 7 shows the average footprint spectra for the four cloud conditions and reveals that DCCs are the brightest clouds and are not affected by water vapor absorption in the near IR, unlike stratus and cirrus clouds. The DCC land spectra are slightly brighter than those over ocean, particularly in the near IR. The standard deviations of the 3253, 340, 16 734, and 1799 SCIAMACHY footprint reflectances for DCC-over-ocean, DCC-over-land, ocean stratus, and cirrus categories, respectively, are shown in Fig. 7. The DCC, stratus, and cirrus footprint spectra have standard deviations of ∼10%, 15%, and ∼40%, respectively, except over the water vapor absorption bands centered at 724, 816, 940, 1140, and 1400 nm [26]. Similar stratus spectra have been observed from aircraft instruments [26]. The DCC spectral signal-to-noise ratio over most of the visible range is an advantage over other cloud conditions for calibration purposes. In order to corroborate the large-footprint SCIAMACHY results, 30-m Hyperion hyperspectral reflectances, obtained from the U.S. Geological Survey archive, are also analyzed.

EO-1 Hyperion, with a local equator crossing time at 10:00 A.M., resolves 220 spectral bands from 0.4 to 2.5 μm at 10-nm increments. The Hyperion 30-m-resolution image dimensions are 7.5 km (cross-track) and 100 km (along track). EO-1 Hyperion is a tasked sensor and does not scan continually. Therefore, imagery must be requested in advance, making it difficult to obtain imagery capturing DCC. Most of the Hyperion imagery is over clear-sky land; however, an (EO1H0180462011300110KF_SGS_01) image over Hurricane Rina in the Gulf of Mexico ($\sim 20^\circ$ N and $\sim 87^\circ$ W) east of the Yucatan Peninsula on October 27, 2011, at 15:50 GMT, with an SZA of 42° and a view angle of 18°, was obtained. Fig. 8 shows the geostationary operational environmental satellites (GOES)-13 IR 4-km-resolution 15:45 GMT image with pixel-level BT less than 205 K shaded in red, which generally defines the hurricane convective core. The Hyperion image boundaries are demarcated by the four blue dots. The corresponding GOES-13 1-km visible image shows the vertical structure of the convection and the cirrus anvil. The actual Hyperion 600-nm image is also shown in the rightmost panel in Fig. 8.

To determine the spectral difference between the convective core and the anvil, the brightest and darkest 10% of the 600-nm pixels are averaged and compared with the mean image spectra and shown in Fig. 9. Remarkably, the brightest Hyperion pixels have a rather low standard deviation of ∼1%. If the reflectance of the top 10% or bottom 10% is divided by the mean image reflectance, the spectral variation between 400 and 1000 nm is less than 1% (not shown). This low variability confirms that DCC can be used to transfer the calibration between sensor channels, which has already been successfully demonstrated [20], [21]. The mean Hyperion image spectra are also compared in Fig. 9 with the SCIAMACHY marine DCC spectra used in Fig. 7. Note the consistency between the spectra, particularly for wavelengths greater than 1 μm. The SCIAMACHY calibration accuracy varies between wavelengths; it is 2% between 0.6 and 0.8 μm, and it is up to 6% between 0.8 and 1.0 μm [27]. The consistency verifies that the large-footprint SCIAMACHY spectra can faithfully reproduce the DCC spectra.

V. Conclusion

DCCs are ideal visible calibration targets because they are very bright nearly isotropic solar reflectors located over the tropics that migrate seasonally with the sun. They have the highest signal-to-noise ratio of any invariant Earth target. They reside at the top of the tropopause, where water vapor absorption is minimal, and they exhibit a near-flat spectral response. Because they can be identified using a simple IR threshold temperature, DCCs offer an opportunity to uniformly calibrate

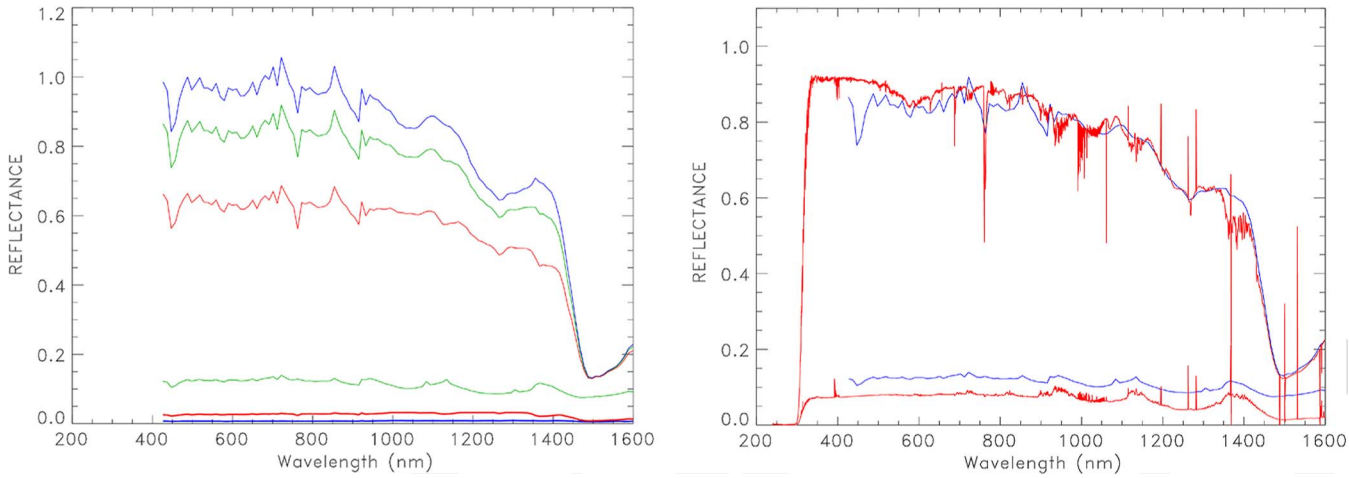

Fig. 9. (Left panel) Mean Hyperion image reflectances for the (blue line) brightest 10% of image and (red line) darkest 10% of image and (green line) full-image mean. The associated standard deviations are the lines plotted between the 0.0 and 0.2 reflectances. (Right panel) (Red line) SCIAMACHY marine DCC footprint reflectances in the top panel in Fig. 7 are overlaid on (blue line) the October 27 15:45 GMT Hyperion mean DCC image spectrum reflectance. The associated standard deviation (red line) SCIAMACHY and (blue line) Hyperion spectrum reflectances are also plotted.

nearly all historical and current visible sensors. A large-ensemble DCC baseline calibration technique was outlined, which was applicable to most historical and current sensors, where the identification of DCC pixels is based on IR BT and spatial uniformity thresholds to evaluate the sensor's temporal stability. The DCC radiances are AC using a sensor-specific DCC ADM. On average, over 500 000 Aqua-MODIS pixels are identified as DCC monthly. The collective DCC AC radiances are used to construct monthly PDF statistics. The monthly PDF modes and means are linearly regressed to derive the stability of the Aqua-MODIS sensor, which is found to be 0.48% per decade when using the baseline technique. It was found that a temperature threshold from 195 K to 205 K provided the least uncertainty for the technique. There was an increase in the DCC AC radiance with lower threshold temperatures, implying that a stable IR sensor calibration is needed. The DCCs were found to be nearly isotropic, with the Lambertian ADM only degrading the temporal uncertainty to 0.67%. Maintaining the proper sample size to derive consistent monthly PDFs ensures the success of this technique when optimizing the selection criteria.

The dominant DCC domains, where DCCs occur almost every month, were found over the TWP, Africa, and South America. It was found that the PDF mode statistic reduced both the temporal variability and regional variability of MODIS bands for wavelengths less than 0.65 μm. The lowest DCC AC radiances were found over the TWP, but the highest radiances were not always found exclusively over land. The most regional-consistent DCC AC radiances were found over the dominant land domains. The consistency were $\sim$0.3% regionally and 1% temporally when the technique was applied over 10°-by-10° latitude-by-longitude regions.

For MODIS bands with wavelengths greater than 1 μm, there is a distinct DCC AC radiance land/water difference, with land having a higher radiance. The PDF mean statistic reduced the land–ocean difference by half compared to the mode method for these longer wavelength bands. The DCC technique has the potential to monitor the 2.12-μm-band stability since the DCC AC radiance regional variation is within 0.7%, and has a temporal variation of 1.1% over the dominant land regions.

DCC reflectances were evaluated spectrally using both SCIAMACHY and Hyperion hyperspectral reflectance measurements. The SCIAMACHY reflectances were compared to marine stratus and cirrus clouds. It was noted that the land spectral reflectance was slightly greater than that of ocean, mainly for wavelengths greater than 1 μm. The DCCs were not affected by water vapor absorption in the near IR, unlike the stratus and cirrus clouds, and had an overall reflectance uncertainty of 10% for all wavelengths. The 10% is likely an overestimate given that the SCIAMACHY footprint is 30 by 240 km. The Hyperion hyperspectral DCC reflectances over a hurricane were compared with the SCIAMACHY reflectances and were consistent. The brightest Hyperion targets in the hurricane had a spectral uncertainty of 1%. It was also noted that the ratio of the reflectances over the hurricane was consistent to within 1%.

The regional, temporal, and spectral characterization of DCC reveals that these invariant Earth calibration targets are stable within 0.5% per decade when using a sensor-specific ADM and possibly within 0.3% per decade when the selection criteria are optimized based on Aqua-MODIS 0.65-μm-band radiances.

ACKNOWLEDGMENT

The authors would like to thank J. Xiong and the MODIS team for the assistance with the MODIS data. The MODIS data were obtained from the NASA Langley Distributed Active Archive Center. This study would not have been completed without the SCanning Imaging Absorption SpectroMeter for Atmospheric CartograpHY (SCIAMACHY) data provided by the European Space Agency Envisat program. The authors would also like to thank J. Burrows, S. Noel, and K. Bramstedt at Bremen University and R. Snel at the Netherlands Institute for Space Research for the assistance with the SCIAMACHY

data. The Hyperion data were obtained from the U.S. Geological Survey.

REFERENCES

[1] P. Abel, "Clouds as calibration targets for AVHRR reflected-solar clouds: Results from a two-year study at NOAA/NESDIS," in *Proc. SPIE*, 1991, vol. 1493, pp. 195–206.

[2] S. H. Ham and B. J. Sohn, "Assessment of the calibration performance of satellite visible channels using cloud targets: Application to Meteosat-8/9 and MTSAT-1R," *Atmos. Chem. Phys.*, vol. 10, no. 5, pp. 11 131–11 149, 2010.

[3] A. Okuyama, Outlined algorithm theoretical basis for MTSAT visible calibration for GSICS (liquid cloud method), GSICS ATBD. [Online]. Available: https://gsics.nesdis.noaa.gov/pub/Development/AtbdCentral/MTSAT_vis_vicarious_calibration_outline.pdf

[4] Y. M. Govaerts, A. Arriaga, and J. Schmetz, "Operational vicarious calibration of the MSG/SEVIRI solar channels," *Adv. Space Res.*, vol. 28, no. 1, pp. 21–30, 2001.

[5] Y. B. Hu, B. A. Wielicki, P. Yang, P. W. Stackhouse, Jr., B. Lin, and D. F. Young, "Application of deep convective cloud albedo observation to satellite-based study of the terrestrial atmosphere: Monitoring the stability of spaceborne measurements and assessing absorption anomaly," *IEEE Trans. Geosci. Remote Sens.*, vol. 42, no. 11, pp. 2594–2599, Nov. 2004.

[6] D. R. Doelling, L. Nguyen, and P. Minnis, "On the use of deep convective clouds to calibrate AVHRR data," in *Proc. SPIE 49th Ann. Mtg., Earth Observ. Syst. IX Conf.*, Denver, CO, Aug. 2–6, 2004, pp. 281–299.

[7] H. H. Aumann, T. Pagano, and M. Hofstadter, "Observations of deep convective clouds as stable reflected light standard for climate research: AIRS evaluation," in *Proc. SPIE*, 2007, vol. 6684, pp. 1–7.

[8] P. Minnis, D. R. Doelling, L. Nguyen, W. Miller, and V. Chakrapani, "Assessment of the visible channel calibrations of the TRMM VIRS and MODIS on Aqua and Terra," *J. Atmos. Ocean. Technol.*, vol. 25, no. 3, pp. 385–400, 2008.

[9] D. R. Doelling, D. Morstad, R. Bhatt, and B. Scarino, "Algorithm Theoretical Basis Document (ATBD) for deep convective cloud (DCC) technique of calibrating GEO sensors with Aqua-MODIS for GSICS," GSICS, 2011. [Online]. Available: http://gsics.nesdis.noaa.gov/pub/Development/AtbdCentral/GSICS_ATBD_DCC_NASA_2011_09.pdf

[10] B. Fougnie and R. Bach, "Monitoring of radiometric sensitivity changes of space sensors using deep convective clouds: Operational application to PARASOL," *IEEE Trans. Geosci. Remote Sens.*, vol. 47, no. 3, pp. 851–861, Mar. 2009.

[11] B. J. Sohn, S.-H. Ham, and P. Yang, "Possibility of the visible-channel calibration using deep convective clouds overshooting the TTL," *J. Appl. Meteorol. Climatol.*, vol. 48, no. 11, pp. 2271–2283, Nov. 2009.

[12] A. Wu, X. Xiong, D. R. Doelling, D. L. Morstad, A. Angal, and R. Bhatt, "Characterization of Terra and Aqua MODIS VIS, NIR, and SWIR spectral band calibration stability," *IEEE Trans. Geosci. Remote Sens.*, vol. 51, no. 6, Jun. 2013, to be published. [Online]. Available: http://ieeexplore.ieee.org

[13] P. Minnis, L. Nguyen, D. R. Doelling, D. F. Young, W. Miller, and D. P. Kratz, "Rapid calibration of operational and research meteorological satellite imagers. Part II: Comparison of infrared channels," *J. Atmos. Ocean. Technol.*, vol. 19, no. 9, pp. 1250–1266, Sep. 2002.

[14] N. G. Loeb, N. Manalo-Smith, S. Kato, W. F. Miller, S. K. Gupta, P. Minnis, and B. A. Wielicki, "Angular distribution models for top-of-atmosphere radiative flux estimation from the Clouds and the Earth's Radiant Energy System instrument on the Tropical Rainfall Measuring Mission satellite. Part. 1: Methodology," *J. Appl. Meteorol.*, vol. 22, no. 4, pp. 338–351, Apr. 2005.

[15] T. Yuan and Z. Li, "General macro- and microphysical properties of deep convective clouds as observed by MODIS," *J. Clim.*, vol. 23, no. 13, pp. 3457–3473, Jul. 2010.

[16] G. Hong, G. Heygster, J. Notholt, and S. A. Buehler, "Interannual to diurnal variations in tropical and subtropical deep convective clouds and convective overshooting from seven years of AMSU-B measurements," *J. Clim.*, vol. 21, no. 17, pp. 4168–4189, Sep. 2008.

[17] H. Shimazaki and S. Shinomoto, "A method for selecting the bin size of a time histogram," *Neural Comput.*, vol. 19, no. 6, pp. 1503–1527, Jun. 2007.

[18] M. K. Yamamoto, F. A. Furuzawa, A. Higuchi, and K. Nakamura, "Comparison of diurnal variations in precipitation systems observed by TRMM PR, TMI, and VIRS," *J. Clim.*, vol. 21, no. 6, pp. 4011–4028, Aug. 2008.

[19] R. Bhatt, D. R. Doelling, D. Morstad, B. R. Scarino, and A. Gopalan, "Desert-based absolute calibration of successive geostationary visible sensors using a daily TOA radiance model," 2012, submitted for publication.

[20] E. F. Vermote and Y. J. Kaufman, "Absolute calibration of AVHRR visible and near infrared channels using ocean and cloud views," *Int. J. Remote Sens.*, vol. 16, no. 13, pp. 2317–2340, 1995.

[21] B. Lafrance, O. Hagolle, B. Bonnel, Y. Fouquart, and G. Brogniez, "Interband calibration over clouds for POLDER space sensor," *IEEE Trans. Geosci. Remote Sens.*, vol. 40, no. 1, pp. 131–142, Jan. 2002.

[22] H. Bovensmann, J. P. Burrows, M. Buchwitz, J. Frerick, S. Noël, V. V. Rozanov, K. V. Chance, and A. P. H. Goede, "SCIAMACHY: Mission objectives and measurement modes," *J. Atmos. Sci.*, vol. 56, no. 2, pp. 127–150, Jan. 1999.

[23] J. Skupin, S. Noël, M. W. Wuttke, M. Gottwald, H. Bovensmann, M. Weber, and J. P. Burrows, "SCIAMACHY solar irradiance observation in the spectral range from 240 to 2380 nm," *Adv. Space Res.*, vol. 35, no. 3, pp. 370–375, 2005.

[24] G. Lichtenberg, Q. Kleipool, J. M. Krijger, G. van Soest, R. , L. G. Tilstra, J. R. Acarreta, I. Aben, B. Ahlers, H. Bovensmann, K. Chance, A. M. S. Gloudemans, R. W. M. Hoogeveen, R. Jongma, S. Noël, A. Piters, H. Schrijver, C. Schrijvers, C. E. Sioris, J. Skupin, S. Slijkhuis, P. Stammes, and M. Wuttke, "SCIAMACHY level 1 data: Calibration concept and in-flight calibration," *Atmos. Chem. Phys.*, vol. 6, no. 12, pp. 5347–5367, 2006.

[25] P. Minnis, S. Sun-Mack, D. F. Young, P. W. Heck, D. P. Garber, Y. Chen, D. A. Spangenberg, R. F. Arduini, Q. Z. Trepte, W. L. Smith, J. K. Ayers, S. C. Gibson, W. F. Miller, G. Hong, V. Chakrapani, Y. Takano, K.-N. Liou, Y. Xie, and P. Yang, "CERES edition-2 cloud property retrievals using TRMM VIRS and Terra and Aqua MODIS data, Part I: Algorithms," *IEEE Trans. Geosci. Remote Sens.*, vol. 49, no. 11, pp. 4374–4400, Nov. 2010.

[26] B. C. Kindel, P. Pilewskie, K. S. Schmidt, O. Coddington, and M. D. King, "Solar spectral absorption by marine stratus clouds: Measurements and modeling," *J. Geophys. Res.*, vol. 116, no. D10, pp. D10203-1–D10203-16, 2011.

[27] "Disclaimer for SCIAMACHY IPF 7.04 Level 1b Products (SCI_NL__1P)," 2011, PO-RS-MDA-GS-2009 Volume 15 Issue 3L. [Online] Available: https://earth.esa.int/c/document_library/get_file?folderId=24074&name=DLFE-484.pdf

David R. Doelling received the B.S. degree in meteorology from The University of Utah, Salt Lake City, in 1985 and the M.S. degree in atmospheric science from the University of Washington, Seattle, in 1991.

He is currently a Senior Research Scientist with the Climate Science Branch, Langley Research Center, National Aeronautics and Space Administration (NASA), Hampton, VA, where he is the Time Interpolation and Spatial Averaging Sublead for the Clouds and the Earth's Radiant Energy System (CERES) project and responsible for the diurnal averaging and spatial gridding of CERES footprint cloud and radiative flux parameters. He is also a member of the Geostationary Earth Radiation Budget Experiment and Megha-Tropique science teams, projects similar to CERES that measure broadband fluxes. He has studied the orbital sampling errors for proposed satellites as a member of the Climate Absolute Radiance and Refractivity Observatory science definition team. He is the Global Space-Based Inter-Calibration System NASA Representative and the Lead for geostationary/MODIS ray-matching and deep convective cloud visible calibration methods. His research interests include geostationary imager calibration, diurnal averaging techniques of satellite observations, and satellite sampling studies.

Daniel Morstad received the B.S. and M.S. degrees in electrical engineering from South Dakota State University, Brookings, in 2007 and 2009, respectively. His graduate research focused on development of a statistically based automation technique for selecting the most temporally invariant Earth targets based on the Landsat-5 Thematic Mapper data record.

He is currently a Research Scientist with Science Systems and Applications, Inc., Hampton, VA, in support of the Clouds and the Earth's Radiant Energy System project at NASA-Langley Research Center, National Aeronautics and Space Administration, Hampton. He is primarily responsible for maintaining the real-time geostationary visible sensor calibration record and is currently developing a deep convective cloud absolute calibration technique that will be vital to the uniform radiometric calibration of both past and future Earth-observing sensors.

Benjamin R. Scarino received the M.S. degree in meteorology from the Pennsylvania State University, State College, in 2010.

He is currently a Staff Research Scientist with Science Systems and Applications, Inc., Hampton, VA. There, he supports the Clouds and the Earth's Radiant Energy System project, working on cloud and radiation data-set development and on-orbit calibration.

Rajendra Bhatt received the B.S. degree in electronics engineering from Tribhuvan University, Kathmandu, Nepal, in 2002 and the M.S. degree in electrical engineering from South Dakota State University (SDSU), Brookings, in 2009.

At SDSU, he has studied the long-term radiometric stability of and calibrated the Landsat-1 through Landsat-5 Multispectral Scanner sensors using pseudoinvariant calibration sites. He is currently a Research Scientist with Science Systems and Applications, Inc., Hampton, VA, in support of the Clouds and the Earth's Radiant Energy System project in Langley Research Center, National Aeronautics and Space Administration, Hampton, where he is developing techniques for in-flight calibration of satellite visible and infrared observations to assess the sensor's performance on orbit and ensure the usability of climate data.

Arun Gopalan received the B.S. degree in mechanical engineering from the Victoria Jubilee Technical Institute, University of Bombay, Mumbai, India, in 1991 and the M.S. degree in mechanical engineering from The State University of New York, Stony Brook, in 1993. He completed all the Ph.D. requirements excluding dissertation defense at The State University of New York in 1997. His dissertation focused on the research and development of an optimal retrieval algorithm for simultaneous extraction of diurnal stratospheric nitrogen dioxide and aerosol extinction profiles using Earth-limb infrared emission measurements from the National Aeronautics and Space Administration (NASA)'s Upper Atmospheric Research Satellite Cryogenic Limb Array Etalon Spectrometer instrument.

He is currently a Senior Research Scientist with Science Systems and Applications Inc., Hampton, VA, in support of the Clouds and Earth's Radiant Energy System and Climate Absolute Radiance and Refractivity Observatory projects at NASA Langley Research Center. He has previously coauthored a number of journal papers and worked in the area of satellite remote sensing for over 15 years with Earth science research groups in the Goddard Space Flight Center, NASA, Greenbelt, MD, and in the National Center for Atmospheric Research, Boulder, CO. His research interests include studies of postlaunch calibration techniques to understand satellite sensor performance, science retrieval algorithm development, remotely sensed data processing methods, aerosol–cloud–climate feedback mechanisms, visualization of large-scale Earth science data sets, and data mining.